Peer-reviewed version available at *Sensors* **2019**, *19*, 3037; doi:10.3390/s19143037

Article

The Young interferometer as optical system for variable depolarizer characterization

Aleksandra Kalbarczyk, Leszek R. Jaroszewicz *, Noureddine Bennis, Monika Chruściel, Paweł Marć

Faculty of Advanced Technologies and Chemistry, Military University of Technology, Warsaw, Poland; aleksandra.kalbarczyk@wat.edu.pl (A.K.), jarosz@wat.edu.pl (L.R.J.), noureddine.bennis@wat.edu.pl (N.B.), monika.chrusciel@wat.edu.pl (M.C.), pawel.marc@wat.edu.pl (P.M.)

* Correspondence: jarosz@wat.edu.pl; Tel.: +48 261 839 014

Received: date; Accepted: date; Published: date

Abstract: In a depolarizing instrument, such as a broadband imaging spectrometer, the depolarizers are placed on the system for stabilization the optical signal. They are also used to reduce measurements offsets due to strong polarization dependence, which produce drastic deterioration of the signal to noise ratio. Dynamic depolarizer with a controllable degree of polarization is also required to study the effect of noise on quantum information. The article described a new instrument for characterization the variable depolarizer with features which make it different from a polarimetric system. The analysing system based on the simple structural design and has good stability for real-time measurement. A practical application of the described interferometer system for variable depolarizer characterization is also presented.

Keywords: Young interferometer; depolarization measurement; modulation of depolarization; liquid crystal device

---

1. Introduction

Interference is a special example of the superposition principle. When two or more propagating coherent waves are incidents on the same point, the resultant amplitude is equal to the vector sum of the amplitudes of the propagating waves. The consequence of the superposition principle can be observed as dark and bright stripes, and their distribution called as fringe pattern. In 1802 Thomas Young performed the first experiment with interference between waves from two similar slits illuminated by a single source of the light (double-slit Young's interferometer). Thenceforth interferometers have found many technical applications. Regards they high accuracy and due to the non-destructive property are often used for instance in medical diagnostics as optical coherence topography instruments [1-2], blood flow [3], middle ear [4] or infectious diseases [5].

The interferometric measurement methods based on comparing images obtained from a charge-coupled device(CCD camera) were proposed, also [6, 7]. They use a single CCD camera and phase is calculated at every single pixel to give a phase map. From other side methods based on a comparison of fringe pattern photos are limited. Complicated algorithms are supported to give a value of the phase shift at each pixel, which is calculated with the help of neighbouring pixels. In works [8-9], Mach–Zehnder interferometer configuration have been used with a single photodetector. A quadrant photodetector and similar to the above technique was proposed to measure the angular position of a parallel laser beam with an interferometric precision [10]. In previously work, we proposed two-channel photodetector in Young interferometer using He-Ne laser as a source of the light. The measurement itself is relative to the measurement using a CCD camera, less time-consuming and does not require the use of complex algorithms. This is a completely new tool for phase measurements adapted for liquid crystal (LC) materials [11].

Another interesting feature of a speckle is it polarization properties study. Polarization speckle pattern consists of a constant polarization state in a reference beam and a random vector phasor sum corresponding to the field scattered from an object in a second beam. Studying the polarization changes of the light caused by a scattering media with a known initial state of the polarization of the incident light is of great interest. The theoretical and experimental studies of polarization speckles for different applications can be found in multiple papers [12-15]. All above applications use polarized light with well-defined state of polarization (SOP) for their proper works according to Fresnel -Arago conditions.

However many optical applications often require depolarized light. For instance in such instrument as an optical spectrum analyzer, polarized incident light is strongly undesirable [16]. The natural light is unpolarized light as well as light from thermal or gas sources. The unpolarized light can be defined as light which vibrations of electric field take place randomly in directions perpendicular to the direction of the wave propagation. According to this definition unpolarized light is light for which the time averages of polarization component become equal to zero. Thus, when the unpolarized light is transmitted through a polarizer, polarized light can be obtained with constant efficiency. In contrast, depolarized light is obtained from polarized or partial polarized light by special devices such as Lyott, Handle or Cornu depolarizer. It can be treated as the composition of two component of equal intensity but contrary SOPs - two linear and perpendicular SOPs, circular left and right SOPs or general two elliptical SOPs with perpendicular azimuths and opposite circulation.

In this extended paper regarding the manuscript showed on I3S 2019: 7th International Symposium on Sensor Science (I3S 2019) [17] we present an interferometric optical system for variable depolarizer characterization, possesses the ability to study variable optical phenomena in real time. We shall, therefore, be concerned with the SOP and the intensity of the light as it passes through the variable depolarizer utilize a liquid crystal (LC) material.

2. Liquid crystal variable depolarizer

The polarization state of the light can be described by the Stokes parameters S_0, S_1, S_2, S_3. Then, the degree of polarization (DOP) can be expressed as:

$$DOP = \frac{\sqrt{S_1^2 + S_2^2 + S_3^2}}{S_0^2} \qquad (1)$$

Depolarization effects can be related to spatially varying birefringent media, where DOP of a partially coherent light decreases during propagation in the medium. Moreover, when a perfectly polarized light beam passes through a depolarizing element, the light beam can be described as a contiguous spatial distribution of a certain number of light beams, which are differently modulated by the local birefringence.

The most known method of depolarizing light is the dispersion of light on porous structures [18]. In these cases, we can observe optical losses inherently associated with light scattering. To avoid losses, other methods of depolarization of light were investigated. Many works investigated LC depolarizing properties [19-21], but there are still a lot of problems in this technology, as instability of depolarizer with time or low depolarizing properties for sources with high coherence length. In present work, we have proposed a depolarizing LC material with specific alignment layers. The most detailed description of depolarizer is given by A. Shaham [22, 23]. All successful designs have been based on his works, in which the depolarizer scheme is composed of a sequence of birefringent crystals and wave plates. The wave plates were used instead of direct rotation of the crystal to eliminate an unwanted angle dependent retardation. These methods suffer from bulkiness and high cost.

LCs are functional materials possessing anisotropies originating from their inner molecular alignment. At a nematic substrate interface as depicted in Figure 1, the tilt angle α is defined as the angle between the easy axis of the nematic molecules and the normal to the surface. Depending on the tilt angle, the alignment of the nematics can be categorized into two major groups: parallel (planar) or perpendicular (homeotropic) alignment. In the first, the easy axis is parallel to the plane

Preprints (www.preprints.org) | NOT PEER-REVIEWED | Posted: 6 May 2019 doi:10.20944/preprints201905.0047.v1

Peer-reviewed version available at Sensors 2019, 19, 3037; doi:10.3390/s19143037

of the surface (the tilt angle is α = 90°), whereas in second - the easy axis is vertical to the surface (α = 0°). For optimum operation of variable depolarizer based on LC, a vertically aligned nematic (VAN) LC with α = 0° pretilts (Figure 1) was proposed. In the off state (voltage V = 0) is isotropic for light impinging at normal incidence. However, the LC molecules orientation upon electric switching ($V \neq$ 0) is undefined; therefore, the cell generates disordered birefringent medium related to undefined switching direction of molecules which produce random polarization of the transmitted light. Therefore depolarization effect is produced [24]. The symmetrical construction of the cell assures that the performance will be the same for light coming from either side. The treatment of problems involving depolarization of incident polarized light beam passing through a variable depolarizing medium and general physical phenomena associated with it is the main element of our investigation. A suitable tool for this treatment is previously reported Young's interferometer [25] constructed with a new principle including the possibility to control the fringe pattern in real time with the objective to study the dynamics of polarization fluctuation.

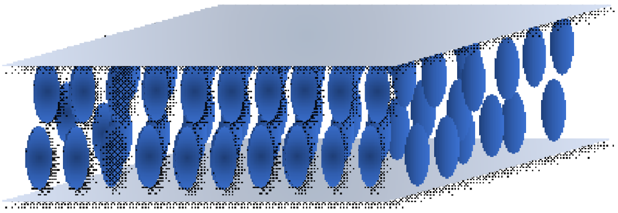

Figure 1. Homeotropic alignment in nematic LC cell.

3. The manufacturing process of the variable depolarizer

In our work, we have proposed a vertical aligned nematic liquid crystal cell as VAN depolarizer (VAND) which uses 15 μm thickness cell filled with LCs having negative dielectric anisotropy. Normally used conventional alignment layer induces a small pretilt in the vertical orientation angle. Such VAN LC cell sandwiched between two crossed polarizers and orientated 45° concerning the polarizer, is isotropic for light impinging at normal incidence when no voltage is applied to the cell. After applying a voltage to the cell, preferred switching direction in VAN cell occurs, thus favoring a specific switching plane. Therefore homogenous switching can be obtained. However, the organic alignment layers like deoxyribonucleic derivatives crosslinked with surfactant complex such as hexadecyltrimethylammonium chloride allow to obtain a vertical arrangement of LC molecules with a non-pretilt (α = 0°). In this case, the LC orientation upon electric switching is undefined; therefore, the cell generates chaotic structures. This produces the depolarization of the incident polarized light because the switching direction of molecules is undefined and VAND is obtained.

To provide the polarization properties of the VAND, it is highly desirable known as the Stokes vector of the transmitted light. Then the depolarization capability of the device for different SOPs of the incident beam can be determined. To analyze the dependence of polarization properties of the light passing through the VAND and to provide the full characterization of LC, the device should be inserted into the special setup for polarization measurement. This setup must see unchanged light intensity for any generated SOP. To maintain the intensity constant during the experiment, a combination of a polarizer and a quarter-wave plate as a polarization state generator (PSG) has been used [26]. As a detector, we implemented a polarimetric head to measure Stokes parameters, power as well as DOP. During the measurements, VAND was inserted between PSG and polarimeter, where the PSG enabled generation of the six input SOPs. For each of the six different SOPs, the Stokes vector of the light transmitted by VAND is measured by the polarimeter. Therefore, the DOP for VAND can be determined with high accuracy as is shown in Figure 2 for different input SOP [26]. These results show that with increasing voltage applied on structure, the DOP of transmitted light decreasing because cell generates disordered birefringent medium related to undefined switching direction of molecules. This phenomenon produces random polarization of the transmitted light. The proposed VAND transmits the polarized component of incident light with a minimum DOP equal about 0.08 for horizontal or ±45 degree linear input SOP at 5.2 V or 4.0 V, respectively. In such

Preprints (www.preprints.org) | NOT PEER-REVIEWED | Posted: 6 May 2019 doi:10.20944/preprints201905.0047.v1

Peer-reviewed version available at *Sensors* **2019**, *19*, 3037; doi:10.3390/s19143037

situation minimum intensity loss and scattering is observed. It is also worth to mention that the orientation of the depolarizer cell doesn't have an impact on obtained measurements.

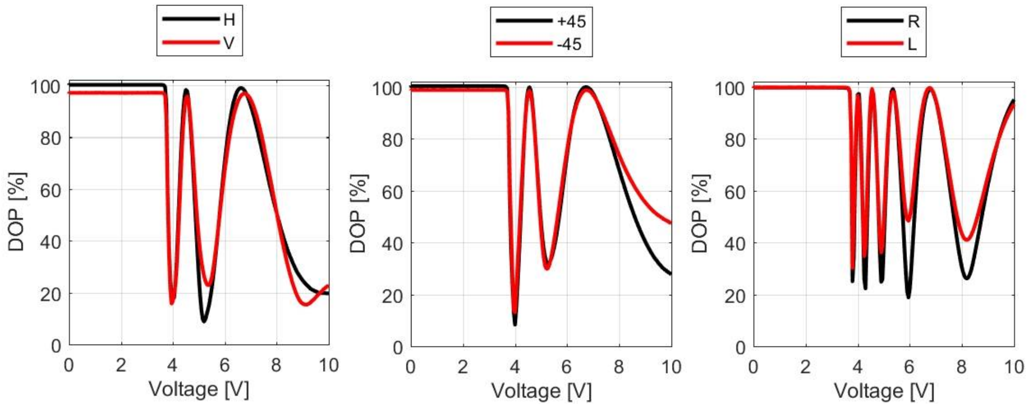

(**a**) (**b**) (**c**)

Figure 2. Measurement results of the DOP for VAND as a function of applied voltage for different input SOP: (a) linear horizontal (H) and vertical (V), (**b**) linear with angle ± 45 deg. Respect to V, (**c**) circular right (R) and left (L).

3. Calibration and essential parameters of the applied interferometric measurement setup

We have investigated the intensity pattern of the light transmitted by VAND using mentioned above interferometer technique in experimental setup shown in Figure 3. The light from a He-Ne laser (λ=633 nm) passes through the polarizer (P) and is spatially filtered (SF) and collimated by a lens (L_1). Next, the light is splitting into two beams by the beam splitter (BS_1). The reference beam is reflected by a mirror (M_1), and a probe beam is reflected by a mirror (M_2). In both paths, telescopes consisting of two positive lenses were inserted to obtain a 400 μm diameter collimated beams. To adjust the equality of the diameter of the reference beam and the probe beam, two collimators with circular pinhole diameter were situated after telescopes. For depolarization properties characterization we have implemented a quarter-wave plate (QP) and a half-wave plate (HP) to generate six SOPs. Then, a right-angled gold coated prism bends the light coming from the collimators by 90°. Thus, the reflected beams become parallel to each other. To adjust the size of the beam, we implemented pinholes (PH), which are placed after telescopes (T) in the system.

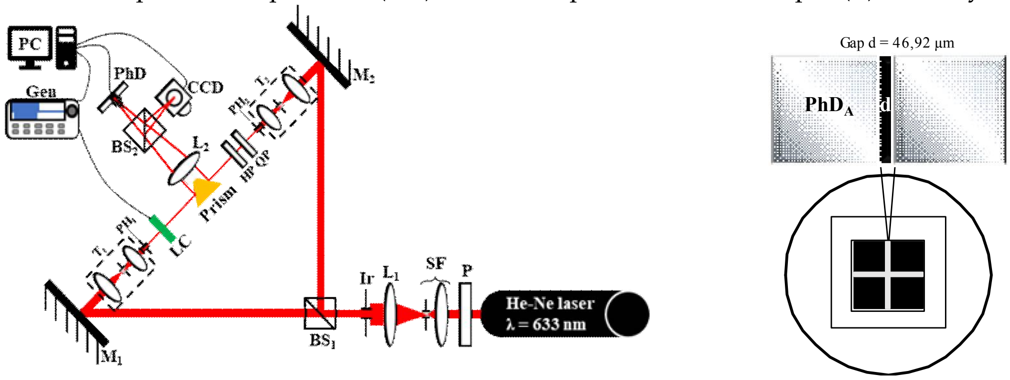

(**a**) (**b**)

Figure 3. The scheme of the interferometer setup: (**a**) general view, (**b**) the scheme of used PhD. Light source: He-Ne laser with λ = 633 nm; P - linear polarizer; SF - spatial filter; Ir – iris, BS - beam splitters; M - mirrors; T – telescopes, PH - pinholes; LC - liquid crystal cell; L_1, L_2 – lenses; PhD – photodetector, Gen – generator, HP – half-wave plate, QP – quarter-wave plate.

The distance between two-point sources and the distance between two photodetectors significantly affects the performance of our setup. Due to the fact, that the distance between two photodetectors is fixed, the calibration process requires the adjustment of the distance between two rays, which is affected by the position of the prism. If the position of the prism is changed, the intensities collected by photodetectors also change. Those intensities are collected in an acquisition card (DAC). LabVIEW software was prepared to record the data. Intensities from PhD_A (I_A) and PhD_B (I_B) are added or subtracted to each other:

$$Sum = I_A + I_B, \qquad Diff = I_A - I_B \tag{2, 3}$$

In reference [24], the detected signals are described as follows:

$$S_R = a_1 + a_2 \cos\Delta\varphi - a_3 \sin\Delta\varphi \qquad S_L = a_1 + a_2 \cos\Delta\varphi + a_3 \sin\Delta\varphi \tag{4, 5}$$

where S_L, S_R are the signals from the left and the right detectors, respectively and $\Delta\phi$ is a phase shift. Those signals depend on the combination of cosine and sine of the measured phase shift. Coefficients a_1, a_2, a_3 are constants depending on the wavelength, the distance between two beams d, the focal length f of the Fourier lens and the size of the beam s and can be calculated from:

$$a_1 = C \int_{d/2}^{\infty} \int_{-\infty}^{\infty} A^2(\rho)\, dy_f\, dx_f \tag{6}$$

$$a_2 = C \int_{d/2}^{\infty} \int_{-\infty}^{\infty} A^2(\rho) \cos\left(\frac{4\pi d x_f}{\lambda f}\right) dy_f\, dx_f \tag{7}$$

$$a_3 = C \int_{d/2}^{\infty} \int_{-\infty}^{\infty} A^2(\rho) \sin\left(\frac{4\pi d x_f}{\lambda f}\right) dy_f\, dx_f \tag{8}$$

where: $A^2(\rho)$ is the spatial distribution of amplitude in the Fourier plane, λ is the wavelength, d is the distance between two beams and f is a focal length of the Fourier lens and C is a constant value. Then, using the relationship describing the signals from the left and right side, the sum $Sum = (S_R + S_L)$ and the difference $Diff = (S_R - S_L)$ can be expressed as:

$$Sum(\Delta\varphi) = 2a_1 + 2a_2 \cos\Delta\varphi \qquad Diff(\Delta\varphi) = 2a_3 \sin\Delta\varphi \tag{9, 10}$$

According to equations (9), (10) a_1 is the amplitude of the sum function, a_2 is the average value of the sum function, and a_3 is the average value of the difference function. To determine the phase difference between the two beams we need to know the sum and the difference of the signal values of coefficients a_1, a_2, and a_3:

$$Sum(\Delta\varphi) = 2a_1 + 2a_2 \cos\Delta\varphi \qquad Diff(\Delta\varphi) = 2a_3 \sin\Delta\varphi \tag{11, 12}$$

The information about an error of the phase difference, induced by this system was analysed and described in reference and had the following expression [25]:

$$\varepsilon = \frac{\rho - 1}{2} \sin(2\Delta\varphi) \tag{13}$$

where: $\varrho = a_3/a_2$. According to equation (13), in the case of $\varrho=1$ the error is equal to zero. Those results indicate that, when $a_3 = a_2$, the error is not dependent on the phase difference value.

Calibration of the setup was performed using a piezoelectric mirror to induce a phase demodulation only in one arm of the interferometer. Results of phase demodulation as a function of time for three different positions of the prism is presented in Figure 4. The variation of the distance between two beams has a significant impact on coefficients a_1, a_2 and a_3, as well as on the quality of the performance of our device [Figure 4(a)]. At the same time in the case where: $a_2 = a_3$ experimental results are in good agreement with the theoretical model [Figure 4(b)].

Peer-reviewed version available at *Sensors* **2019**, *19*, 3037; doi:10.3390/s19143037

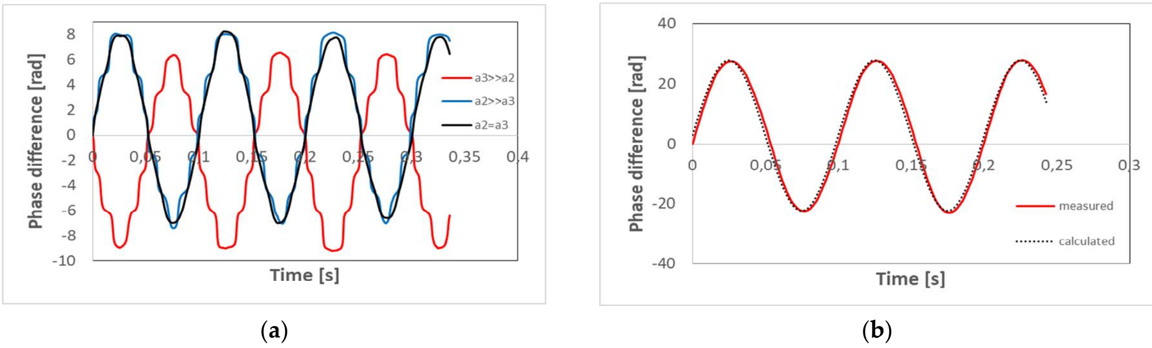

Figure 4. System adjustment: (**a**) Dynamic phase shift measurements at three different values of the distance between two beams *d*., (**b**) Comparison of the theoretical model (dotted line) and measured phase shift when coefficients a_2 and a_3 are equal.

4. Dynamic behavior of depolarizer VAND

The optical system, calibrated according to the procedure described above, performs an interferometric analysis for the spatial distribution of varying polarization in cross section of the depolarized beam transmitted by VAND. A more desirable depolarizer would operate with varying applied voltage. In the case of VAND, the applied waveform is sketched in Figures 5(a) and 6(a). The voltage pattern applied to VAND was 1 kHz AC voltage modulated by 10 Hz envelope with amplitude of 9 V [Figure 5(a)] and 50 Hz envelope with an amplitude of 7 V [Figure 6(a)]. We have measured with the investigation of an impact of the SOP of the reference beam on the depolarization capability of VAND. The beams in both arms are adjusted in such a way that their intensities are equal on recombination. In Figure 5(b) we have compared obtained response of VAND for the waveform shown in Figure 5(a).

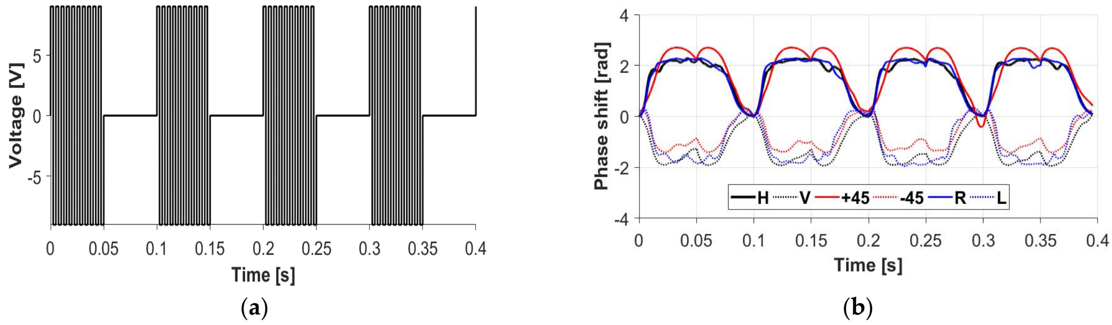

Figure 5. The results of VAND investigation: (**a**) The voltage pattern applied to LC device (1 kHz AC voltage modulated by 10 Hz envelope with 9 V amplitude), (**b**) phase demodulation caused by VAND is driven by a signal (**a**) obtained for six SOPs measured for this waveform.

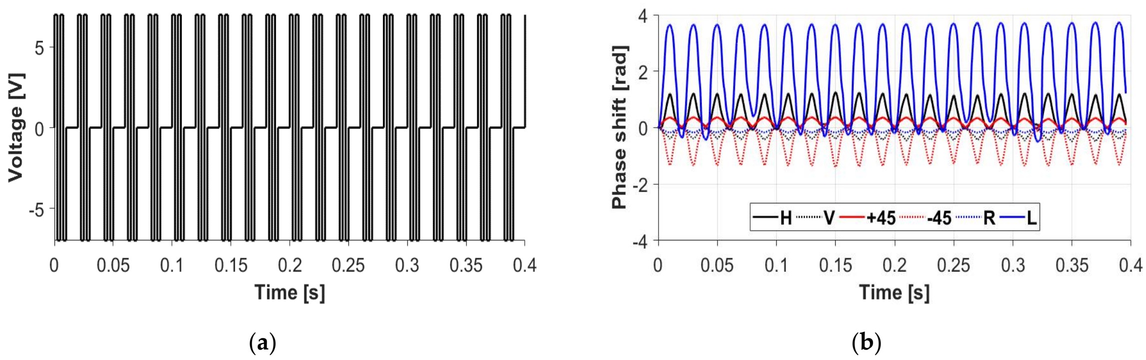

Figure 6. The results of VAND investigation: (**a**) the voltage pattern applied to LC device (1 kHz AC voltage modulated by 50 Hz envelope with 7 V amplitude), (**b**) phase demodulation caused by VAND is driven by a signal (a) obtained for six SOPs measured for this waveform.

For linear polarization, it can be noticed that the modulation depth is comparable for opposite SOPs, i.e., horizontal and vertical or +45° and -45°of the reference beam. However, the sign of the phase shift is different. This result reflects the correlation between orthogonal equal-intensity electric field components at a single space-time point. This effect is manifested in Figure 5(b). In this case, the DOP can be considered as the degree of correlation between the orthogonal components which is a fundamental definition of unpolarized light. Increasing the modulation frequency of the applied waveform [Figure 6(a)], the performance of the depolarizer has been changed. In this case for circular polarization of the reference beam, we have obtained high demodulation for the circular left; however, for the circular right, there is almost no modulation. Demodulation depth results presented in Figure 6(b) give us information about the contribution of each polarization state caused by the depolarizing device for a certain situation. In our case, the light after passing through VAND device is depolarized maintaining right circular polarization the most dominant in the cross-section of the beam.

This method implemented to investigate the polarization properties can give us new information about tested depolarizer, which cannot be observed by standard methods. From the analysis of the results of Figure 5(b) we conclude that the light transmitted by the investigated VAND is totally depolarized, whereas in the case of Figure 6(b) is partially depolarized. This result establishes a new, interferometric interpretation for the DOP of the unpolarized beam.

5. Conclusions

We have proposed a new approach of interpretation of the DOP directly from interference obtained by Young interferometer setup in the time domain. The presented dynamic shift of the interference pattern relates to the phase modulation controlled by VAND shows an ability of VAND to generate polarization modulation when it is driven by modulated signal waveform. The proposed technique can find future application in sensing devices as well as biomedical studies of depolarization caused by different types of media.

Author Contributions: conceptualization, L.R.J., and N.B.; methodology, N.B.; software, P.M..; validation, A.K., N.B., and L.R.J.; formal analysis, A.K.; investigation, M.C..; writing—draft, review and editing, A.K. and L.R.J.

Funding: This research was funded by the Ministry of the National Defence Republic of Poland - Research Grant no. GBMON/13-995/2018/WAT.

Conflicts of Interest: The authors declare no conflict of interest.

References

1. Fercher, A.; Mengedoht, K.; Werner, W. Eye-length measurement by interferometry with partially coherent light. *Opt. Lett.*, **1988**, *13*, 186–188.
2. Huang, D.; Swanson, E.; Lin, C.P.; Schuman, J.; Stinson, W.; Chang, W. Optical coherence tomography. *Science*, **1991**, *254*, 1178–1181.
3. Magnain, C.; Castel, A.; Boucneau, T.; Simonutti, M.; Ferezou, I.; et al., Holographic laser Doppler imaging of microvascular blood flow. *J. Opt. Soc. Am. A*, **2014**, *31*, 2723–2735.
4. Drake, A. Laser interferometry applied to middle ear diagnosis. *Proceedings of the 5th New England Bioengineering Conference*, **1977**, 225-228.
5. Kussrow, A.; Enders, C.; Castro, A.; Cox, D.; Ballard, R.; Bornhop, D. The potential of backscattering interferometry as in vitro clinical diagnostic tool for the serological diagnosis of infectious disease. *Analyst*, **2010**, *135*, 1535-1537.
6. Burke, J. *Application and optimization of the spatial phase shifting technique in digital speckle interferometry*. Carl von Ossietzky University, Oldenburg, Germany, 2000.
7. Bavigadda, V. *A new versatile electronic speckle pattern interferometer for vibration measurements*. Dublin Institute of Technology, Dublin, Ireland, 2008.
8. Clark, T.; Dennis, M. Coherent optical phase-modulation link. *IEEE Photon. Technol. Lett.*, **2007**, *19*, 1206–1208.
9. Fernandes, N.; Gossner, K.; Krisch, H. Low power signal processing for demodulation of wide dynamic range of interferometric optical fibre sensor signals. *Proc. SPIE*, **2010**, *7653*, 765328.

10. Paolino, P.; Bellon, P.L. Single beam interferometric angle measurement. *Opt. Commun.*, **2007**, *280*, 1–9.
11. Bennis, N.; Merta, I.; Kalbarczyk, A.; Maciejewski, M.; Marc, P.; et al. Real time phase modulation measurements in liquid crystals. *Opto-Electron. Rev*., **2017**, *25*, 69–73.
12. Li, J.; Yao, G.; Wang, L. Degree of polarization in laser speckles from turbid media: Implications in tissue optics. *J. Biomed. Opt*., **2002**, *7*, 307–312.
13. Schmidt, M.; Aizpurua, J.; Zambrana-Puyalto, X.; Vidal, X.; Molina-Terriza, G.; Sáenz, J. Isotropically polarized speckle patterns. *Phys. Rev. Lett*., **2015**, *114*, 113902.
14. Zhang S.; Wang, W. Statistical properties of Stokes parameters in polarization speckle generated from a rough surface scattering. *Proc. SPIE*, **2013**, *9066*, 906606.
15. Ghabbach, A.; Zerrad, M.; Soriano, G.; Amra, C. Accurate metrology of polarization curves measured at the speckle size of visible light scattering. *Opt. Express*, **2014**, *22*, 14594-14609.
16. Tai A.; Yu, F.T.S. Synchronous dual-channel optical spectrum analyser. *Appl. Opt*., **1979**, *18*, 1297-1297.
17. Kalbarczyk, A.; Jaroszewicz, L.R.; Bennis, N.; Chrusciel, M.; Marc, P. Optical system for variable depolarizer characterization. Proceedings of the 7th International Symposium on Sensor Science (I3S 2019), Napoli, Italy, 9-11 May 2019, MDPI , https://www.mdpi.com/journal/proceedings
18. Beckmann, P.; Spizzichino, A. *The Scattering of Electromagnetic Waves from Rough Surfaces*, Artech Print on Demand, 1987.
19. Polat, O. Theoretical study on depolarization of the light transmitted through a non-uniform liquid crystal cell. *Optik*, **2016**, *127*, 3560-3563.
20. Vena, C.; Versace, C.; Strangi, G.; Roberto, B. Frédericksz transition in homeotropically aligned liquid crystals: A photopolarimetric characterization. *Phys. Sta. Sol*., **2008**, *5*, 1257-1260.
21. Domański, A.; Budaszewski, D.; Sierakowski, M.; Woliński, T. Depolarization of partially coherent light in liquid crystals. *Opto-Electron. Rev*., **2006**, *14*, 305-310.
22. Shaham, A.; Eisenberg, H. Realizing a variable isotropic depolarizer. *Opt. Lett*., **2012**, *37*, 2643-2645.
23. Shaham, A.; Eisenberg, H. Realizing controllable depolarization in photonic quantum-information channels. *Phys. Rev. A*, **2011**, *83*, 022303.
24. Vena, C.; Massarelli, R.; Carbone, F.; Versace, C. An approach to a model disordered birefringent medium for light depolarization applied to a liquid crystal device. *Journal of Optics*, **2014**, *16*, 1-8.
25. Merta, I.; Hołdyński, Z.; Jaroszewicz, L.R. Bicell-photodetector in the Fourier plane as a fiber optic homodyne phase demodulator: theoretical model and experimental results. *Appl. Opt*., **2013**, *52*, 4468-4476
26. Kalbarczyk, A.; Bennis, N.; Merta, I.; Spadlo, A.; Węglowski, R.; Kwiatkowska, M.; Marć, P.; Jaroszewicz L.R. Modulation of depolarization analyzed by interferometry setup. *Proc. SPIE*, **2018**, *10834*, 10834-89.